

Model for dense granular flows down bumpy inclines

Michel Y. Louge*

Sibley School of Mechanical and Aerospace Engineering, Cornell University, Ithaca, New York 14853, USA

(Received 4 December 2002; published 13 June 2003)

We consider dense flows of spherical grains down an inclined plane on which spherical bumps have been affixed. We propose a theory that models stresses as the superposition of a rate-dependent contribution arising from collisional interactions and a rate-independent part related to enduring frictional contacts among the grains. We show that dense flows consist of three regions. The first is a thin basal layer where grains progressively gain fluctuation energy with increasing distance from the bottom boundary. The second is a core region where the solid volume fraction is constant and the production and dissipation of fluctuation energy are nearly balanced. The last is a thin collisional surface layer where the volume fraction abruptly vanishes as the free surface is approached. We also distinguish basal flows with the smallest possible height, in which the core and surface layers have disappeared. We derive simple closures of the governing equations for the three regions with insight from the numerical simulations of Silbert *et al.* [Phys. Rev. E **64**, 051302 (2001)] and the physical experiments of Pouliquen [Phys. Fluids **11**, 542 (1999)]. The theory captures the range of inclination angles at which steady, fully developed flows are observed, the corresponding shape of the mean and fluctuation velocity profiles, the dependence of the flow rate on inclination, flow height, interparticle friction, and normal restitution coefficient, and the dependence of the height of basal flows on inclination.

DOI: 10.1103/PhysRevE.67.061303

PACS number(s): 45.70.Mg, 45.70.Vn, 45.50.-j, 45.70.Ht

I. INTRODUCTION

The flows of grains down rough inclined planes have served as a model for geophysical phenomena such as rock slides, dunes, and avalanches, in which the base of the flow is irregular on the small scale. Pouliquen and Chevoir [1] wrote a review of past and current research on the subject.

Two studies have shed recent insight on the phenomenon. In the first, Pouliquen [2] conducted a series of experiments with monodisperse glass spheres in a wide chute roughened by gluing similar beads on the base. In the second, Silbert *et al.* [3] ran numerical simulations, in which they recorded profiles of solid volume fraction and of the mean and fluctuation velocity of the grains for different angles of inclination of a bumpy inclined surface.

From these studies, it is clear that steady, fully developed (SFD) flows down a rough plane are generally dense. The roughness of the base frustrates the motion of the grains, thus leading to a vanishing granular velocity there. The movement induced by the gravitational acceleration then shears the entire flow, leading to granular agitation through the whole depth, except at the rough base, where granular agitation is dissipated.

Pouliquen [2] made two principal observations. First, SFD flows only exist within a range of angles of inclination α between the base and the horizontal, $\alpha_{min} < \alpha \leq \alpha_{max}$. These flows have a minimum height normal to the base $h \geq h_{stop}(\alpha)$, which decreases with increasing α . They stop if $h < h_{stop}(\alpha)$ or if $\alpha \leq \alpha_{min}$. They accelerate *ad infinitum* with $\alpha > \alpha_{max}$. Second, Pouliquen showed that the depth-average grain velocity \bar{u} scales as $h^{3/2}$. This result is in

contrast with flows down a flat, frictional incline, where \bar{u} scales as $h^{1/2}$ [4].

Silbert *et al.* [3] presented detailed profiles, from which one can distinguish three regions in the depth of the flow. Near the base, the fluctuation energy of the grains increases to reach a maximum within a few grain diameters from the rough bottom surface. We call this region the basal layer.

Above this layer, the core of the flow is subject to a shear stress that gradually decreases toward the free surface as the weight of the granular overburden diminishes. In this core region, granular agitation is produced from the working of the mean shear through the gradient of the mean velocity. In turn, the agitation endows the grains with a rate-dependent shear stress that is driven by collisional interactions. However, because of the high packing density of the grains, the latter do not only interact through impulsive collisions. They also experience enduring frictional contacts leading to a rate-independent component of the stresses. Remarkably, Silbert *et al.* [3] observed that the core region possesses a volume fraction independent of depth.

The third region is located near the free surface. It is energized by the agitation conducted from the core and by the shearing. Its volume fraction abruptly reaches zero at the free surface. Its thickness is only a few grain diameters. We call it the surface layer.

In this paper, we present a model that captures the observations of Pouliquen [2] and Silbert *et al.* [3]. Our principal hypothesis follows Savage [5] and others in assuming that the stresses have two components. The first is rate dependent. It is driven by collisional interactions and is given by the dense kinetic theory of Jenkins [6] in terms of the granular agitation and the shear rate. The second is rate independent and derives from long-lasting frictional contacts of the grains. In these SFD flows, we further assume that the corresponding enduring shear stress is proportional to the enduring normal stress through a constant friction coefficient μ_E .

*Email address: Michel.Louge@cornell.edu; URL: <http://www.mae.cornell.edu/microgravity/>

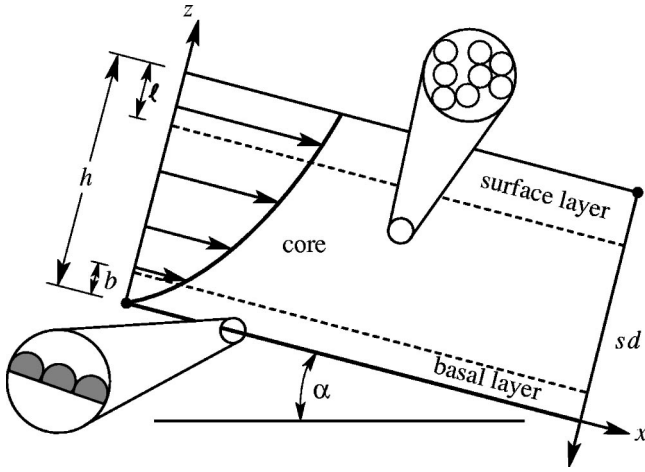


FIG. 1. Sketch of a SFD flow down a bumpy incline showing notation used in the text and the three regions considered in the model.

We begin by writing governing equations for this flow that are consistent with the above hypothesis. We then exploit insight from the numerical simulations of Silbert *et al.* [3] to indicate how these equations can provide closed solutions. Finally, we compare the predictions with the data of Pouliquen [2] and Silbert *et al.* [3].

II. GOVERNING EQUATIONS

We consider flows of monodisperse spherical grains of material density ρ_s . The local state of flow is characterized by the solid volume fraction ν , and by the granular mean and fluctuation velocities, which are made dimensionless with the square root of the grain diameter d and the gravitational acceleration g . The square of the fluctuation velocity is the “granular temperature” $T \equiv (1/3)\langle u'_i u'_i \rangle$, where $u'_i \equiv \tilde{u}_i - u_i$, \tilde{u}_i is the instantaneous velocity, u_i is its average over time, and the index $i = x, y, z$ denotes three orthogonal Cartesian directions pointing, respectively, downward along the flow, across its width and up perpendicularly from the bottom surface (Fig. 1). The granular temperature is a measure of the agitation of the grains.

In SFD flows, the mean velocity is parallel to the base, $u_y = u_z = 0$ and $u_x \equiv u$. Simple force balances on an infinitesimal slice of thickness dz yield differential equations for the shear stress S and normal stress N on surfaces parallel to the base

$$\frac{dS}{dz} = -\rho_s \nu g \sin \alpha, \quad (1)$$

and

$$\frac{dN}{dz} = -\rho_s \nu g \cos \alpha. \quad (2)$$

In a dense flow, these equations can be integrated to yield, approximately,

$$S \approx \rho_s \bar{\nu} g \sin \alpha (h - z) \quad (3)$$

and

$$N \approx \rho_s \bar{\nu} g \cos \alpha (h - z), \quad (4)$$

in which the depth-averaged volume fraction $\bar{\nu}$ was substituted for its local value. The ratio of shear to normal stress represents the effective friction exerted by the grains on adjacent layers parallel to the base. In SFD flows, it is constant and equal to the tangent of the angle of inclination,

$$\frac{S}{N} = \tan \alpha. \quad (5)$$

Our approach is to distinguish two components of the stresses

$$S = S_I + S_E \quad (6)$$

and

$$N = N_I + N_E, \quad (7)$$

where the subscript I refers to impulsive interactions leading to rate-dependent stresses and the subscript E denotes enduring contacts associated with rate-independent stresses. Recent simulations by Campbell [7] indicate that rate-dependent and rate-independent stresses generally coexist. We model the latter by postulating the existence of an internal friction μ_E such that

$$\frac{S_E}{N_E} = \mu_E. \quad (8)$$

For convenience, we define the fraction η of the total shear stress that is rate independent,

$$\eta \equiv \frac{S_E}{S}. \quad (9)$$

Thus, a purely collisional flow like that studied by Jenkins [6] has a stress fraction $\eta = 0$. A static granular heap that is not flowing has $\eta = 1$. In SFD flows, we then combine Eqs. (5)–(9) and express the ratio of any two stresses among S , N , S_I , N_I , S_E , and N_E in terms of η , $\tan \alpha$, and μ_E . For example, the effective collisional friction is

$$\Xi \equiv \frac{S_I}{N_I} = \frac{(1 - \eta) \tan \alpha}{(1 - \eta \tan \alpha / \mu_E)}. \quad (10)$$

To model the rate-dependent stresses, we invoke the theory of Jenkins [6], who assumed that velocity fluctuations and normal stresses are isotropic, and who provided expressions in the limit where ν is large,

$$S_I = a_1 \rho_s \nu^2 g_{12}(\nu) d \sqrt{T} \frac{du}{dz}, \quad (11)$$

where g_{12} is the sphere pair distribution function at contact and $a_1 = 8(1 + \pi/12)/5\sqrt{\pi}$. For such dense flows, we adopt the correction of Torquato [8] to the pair distribution function of Carnahan and Starling [9],

$$g_{12}(\nu) = \frac{2 - \nu}{2(1 - \nu)^3} \quad \text{for } 0 \leq \nu \leq \nu_f \quad (12)$$

and

$$g_{12}(\nu) = \frac{(2 - \nu_f)(\nu_c - \nu_f)}{2(1 - \nu_f)^3(\nu_c - \nu)} \quad \text{for } \nu_f < \nu < \nu_c, \quad (13)$$

where $\nu_f = 0.49$ and $\nu_c = 0.64$ is the random close packing fraction. In this dense limit, the normal collisional stress is

$$N_I = 4\rho_s \nu^2 g_{12}(\nu) T. \quad (14)$$

From Eqs. (11) and (14), it is clear that the rate-dependent stresses are governed by the magnitude of the fluctuation energy. To determine the latter, we write a SFD fluctuation energy balance in an infinitesimal slice of thickness dz ,

$$-\frac{dq}{dz} + (S_I + S_E) \frac{du}{dz} - \gamma = 0. \quad (15)$$

The balance involves a flux of fluctuation energy provided by Jenkins [6] in the dense limit

$$q = -a_2 \rho_s \nu^2 g_{12}(\nu) d \sqrt{T} \frac{dT}{dz}, \quad (16)$$

with $a_2 = 4(1 + 9\pi/32)/\sqrt{\pi}$, and a volumetric rate of energy dissipation

$$\gamma = a_3 \rho_s \nu^2 g_{12}(\nu) T^{3/2}/d, \quad (17)$$

where

$$a_3 = 24(1 - e_{eff})/\sqrt{\pi}, \quad (18)$$

and e_{eff} is an effective coefficient of restitution combining the collisional energy dissipation associated with inelastic and frictional impacts [10]. To derive Eqs. (11), (14), (16), and (17), Jenkins [6] assumed that the collisional fluctuation energy dissipation is small or, equivalently, that e_{eff} is nearly unity.

In Eq. (15), we follow Louge and Keast [4] in allowing both the enduring and impulsive stresses to produce fluctuation energy by their working through gradients of the mean velocity. For flows down a flat, frictional surface, Louge and Keast [4] showed that ignoring the production associated with enduring stresses would lead to restrictions prohibiting the existence of SFD flows for most situations of practical interest.

Jenkins [6] noted that Eq. (15) is a linear ordinary differential equation in the dependent fluctuation velocity variable $w \equiv \sqrt{T}$. He also wrote Eq. (15) in terms of the dimensionless distance $s \equiv (h - z)/d$ from the free surface (Fig. 1). Thus,

combining Eq. (3) through Eq. (18), we obtain three equations governing SFD flows down an inclined plane

$$\frac{d}{ds} \left\{ \left(1 - \frac{\eta \tan \alpha}{\mu_E} \right) s \frac{dw^*}{ds} \right\} - \left\{ \frac{a_3}{2a_2} \left(1 - \frac{\eta \tan \alpha}{\mu_E} \right) - \frac{8 \tan^2 \alpha}{a_1 a_2} \left(\frac{1 - \eta}{1 - \eta \tan \alpha / \mu_E} \right) \right\} s w^* = 0, \quad (19)$$

$$\frac{du^*}{ds} = -\frac{4}{a_1} w^* \tan \alpha \left\{ \frac{1 - \eta}{1 - \eta \tan \alpha / \mu_E} \right\}, \quad (20)$$

and

$$\nu^2 g_{12}(\nu) = \frac{\bar{\nu} \cos \alpha}{4w^{*2}} \left(1 - \frac{\eta \tan \alpha}{\mu_E} \right) s. \quad (21)$$

In these equations the asterisks denote velocities made dimensionless with \sqrt{gd} . Unfortunately, these three equations are not sufficient to determine the four dependent variables u^* , w^* , ν , and η . In order to close this problem, we will exploit insight provided by the numerical simulations of Silbert *et al.* [3] in the three regions of the flow. We begin with the core.

III. THE CORE REGION

In the core, Silbert *et al.* [3] observed that the solid volume fraction is remarkably constant. Because the core spans most of the flow depth, we write that its solid volume fraction is roughly equal to the average throughout the flow

$$\nu_{core} \approx \bar{\nu}. \quad (22)$$

We then determine η using the energy equation, in which we neglect the flux gradient term. Later, once the mean and fluctuation velocities are known through the depth, we will justify this assumption by evaluating the relative magnitude of this term. With this simplification, Eq. (19) reduces to a quadratic equation in η ,

$$\frac{(1 - \eta) \tan^2 \alpha}{(1 - \eta \tan \alpha / \mu_E)^2} = \frac{a_1 a_3}{16}. \quad (23)$$

To possess real solutions, this equation requires

$$\tan \alpha \geq \tan \alpha_{min} = \frac{\mu_E}{1 + 4\mu_E^2/(a_1 a_3)}. \quad (24)$$

The inequality determines the minimum inclination at which SFD flows exist. If it is satisfied, Eq. (23) has two solutions. The larger is typically near unity and gradually increases with angle of inclination. We dismiss it because it is unphysical for the flow to become less collisional with increasing inclination. Then, in the core, we find

$$\eta = \eta_{core} = \mu_E \left\{ \frac{1}{\tan \alpha} - \frac{8\mu_E}{a_1 a_3} \right\} - \frac{4\mu_E}{\sqrt{a_1 a_3}} \sqrt{1 - \frac{\mu_E}{\tan \alpha} + \frac{4\mu_E^2}{a_1 a_3}}. \quad (25)$$

In turn, because $0 \leq \eta < 1$, this expression yields another necessary condition for SFD flows,

$$\tan \alpha \leq \tan \alpha_{max} = \sqrt{a_1 a_3}/4. \quad (26)$$

We then calculate the fluctuation velocity profile from Eqs. (21) and (25),

$$w^*(z) = 2 \sqrt{\frac{\Xi_{core} \sin \alpha}{a_1 a_3 \nu_{core} g_{12}(\nu_{core})}} \sqrt{\frac{h-z}{d}}, \quad (27)$$

where Ξ_{core} is given by Eq. (10) in terms of η_{core} , α , and μ_E . We integrate Eq. (20) to find the corresponding velocity profile

$$u^*(z) = u_b^* + \frac{16}{3a_1} \Xi_{core}^{3/2} \sqrt{\frac{\sin \alpha}{a_1 a_3 \nu_{core} g_{12}(\nu_{core})}} \times \left(\frac{h}{d} \right)^{3/2} \left\{ \left(\frac{h-b}{h} \right)^{3/2} - \left(\frac{h-z}{h} \right)^{3/2} \right\}. \quad (28)$$

We will calculate later the thickness b of the basal layer and the mean velocity u_b where it meets the core. Silbert *et al.* [3] already recognized the general form of the velocity profile in Eq. (28). They derived an expression similar to this equation assuming that the shear stress is proportional to the square of the mean strain rate through a constant to be determined. One contribution of our model is to establish the form of that constant. Another is, like Savage [5], to provide angular limits between which SFD flows can exist.

It remains to determine the volume fraction. Sadly, we do not know how to do so in the core. Fortunately, the solutions in Eqs. (27) and (28) are relatively insensitive to its exact value. Nonetheless, to close the problem, we note that the simulations of Silbert *et al.* [3] suggest the following relation (Fig. 2):

$$\nu_{core} \sim 0.545 + 0.066 \eta_{core}. \quad (29)$$

The simulations imply that, when the volume fraction is near random loose packing, the value of η_{core} tends to zero, and the flow becomes fully collisional, thus losing its SFD character through gradual acceleration. Conversely, a linear extrapolation indicates that the flow will lock up when the volume fraction approaches 61% or so. Further insight from numerical simulations is needed to establish whether the correlation in Eq. (29) has any merit beyond the conditions examined by Silbert *et al.* [3].

Because the core solution predicts a vanishing granular agitation at the free surface [Eq. (27)], it contradicts evidence from the numerical simulations [3]. Thus, the flow near the surface has a different character, which we examine next.

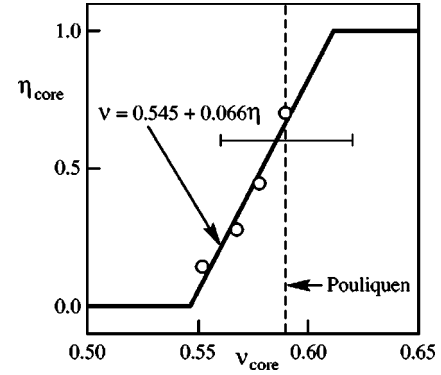


FIG. 2. Stress fraction versus solid volume fraction in the core. The symbols are volume fraction data from model *L3* of Silbert *et al.* [3], in which we evaluate η_{core} using Eq. (25). The lines show a suggested fit through the data. The vertical dashed line indicates Pouliquen's estimate of the mean volume fraction in his experiments and the associated error bar.

IV. THE SURFACE LAYER

The core solution, if extended all the way upward, would, in principle, satisfy the free surface boundary conditions for the flux ($q=0$) and all stresses ($S_E=S_I=N_E=N_I=0$). However, there are several reasons why it is inaccurate near the free surface. First, because the flux gradient from Eqs. (16) and (27) diverges as $z \rightarrow h$, it cannot be balanced by collisional dissipation in Eq. (15). Second, the volume fraction is known to decline from its constant value in the core as the free surface is approached [3]. Third, the core solution stipulates that enduring and collisional stresses remain proportional [Eq. (25)]. However, the form of the granular agitation in Eq. (27) and of the energy flux in Eq. (16) imply that there is a net influx of fluctuation energy from the core to the surface layer. Because the surface layer is sheared through its depth, and because it is the scene of a diminishing solid volume fraction, it is likely to involve mainly collisional interactions. Finally, the simulations indicate that the fluctuation energy does not vanish at the free surface, but instead exhibits an inflexion toward higher values [3]. Thus, it is reasonable to assume that the surface layer has distinct physics from the core region. For these reasons, we assume $\eta=0$ in the surface layer. Numerical simulations should determine whether this assumption has any merit.

With $\eta=0$, the energy equation becomes

$$\frac{d}{ds} \left(s \frac{dw^*}{ds} \right) - k^2 s w^* = 0, \quad (30)$$

in which we define

$$k^2 \equiv \frac{a_3}{2a_2} - \frac{8 \tan^2 \alpha}{a_1 a_2}. \quad (31)$$

Condition (26) guarantees that $k^2 > 0$. In general, solutions to Eq. (30) are modified zeroth-order Bessel functions of the first and second kind, respectively, $I_0(ks)$ and $K_0(ks)$. Because the energy flux vanishes at the free surface, only the Bessel function of the first kind has physical significance. We

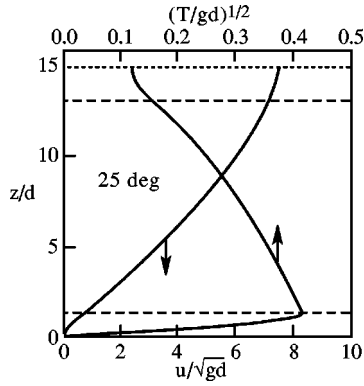


FIG. 3. Typical profiles of dimensionless mean and fluctuation velocities for Pouliquen's "system 1" at the inclination shown. The horizontal dashed lines mark the interfaces between the surface layer, the core, and the basal layer.

solve Eq. (30) by matching the magnitude and slope of w^* at the interface between the core and the surface layer. These two boundary conditions yield the magnitude of the fluctuation velocity profile

$$w^*(s) = \frac{2}{I_0(\lambda_0)} \sqrt{\frac{\bar{\Xi}_{core} \lambda_0 \sin \alpha}{\nu_{core} g_{12} (\nu_{core}) a_1 a_3 k}} I_0(ks), \quad (32)$$

and the depth of the surface layer

$$\ell = \lambda_0 d / k. \quad (33)$$

In these equations, $\lambda_0 \approx 1.07$ is a solution to

$$I_0(\lambda_0) = 2\lambda_0 I_1(\lambda_0), \quad (34)$$

where I_1 is the first-order modified Bessel function of the first kind.

We then determine the mean velocity profile by matching its value at the interface between the core and the surface layer, and by integrating Eq. (20) numerically with $\eta=0$. Finally, we evaluate the profile of solid volume fraction by substituting the fluctuation velocity (32) in the equation of state (21) with $\eta=0$ and by solving the resulting equation in ν . Figures 3 and 4 show typical profiles through the depth, including the basal layer discussed in the following section.

Because in this simple approach there is a discontinuity of η at the interface between the core and the surface layer, neither the slope of the mean velocity profile nor the volume fraction are continuous there (Fig. 4). This defect is small and without much consequence when evaluating integrals leading to the depth-averaged velocity or the overall mass flow rate. One may artificially eliminate the discontinuity by substituting η_{core} for $\eta=0$ in Eq. (21) before calculating the volume fraction profile.

Note that, because in this model the volume fraction vanishes abruptly at the free surface (Fig. 4), it is legitimate to assume a form for the governing equations that is appropriate for dense flows, rather than invoking more complicated expressions that would span the entire range of solid volume fractions.

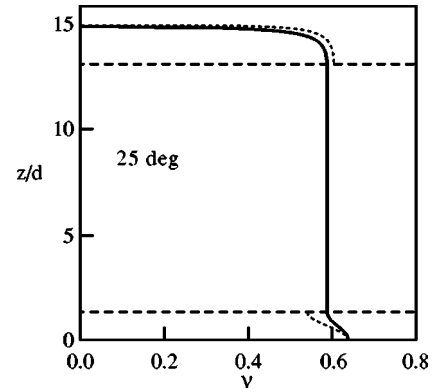


FIG. 4. Profile of solid volume fraction for the conditions of Fig. 3. The dashed curves denote the volume fractions calculated from Eq. (21) with the value of η predicted by the model. The solid lines represent curves in which discontinuities have been removed by artificially adopting $\eta = \eta_{core}$ in Eq. (21) for the surface and basal layers.

Finally, we can now evaluate the error involved in neglecting the flux gradient term in our determination of η in the core. Using the profiles of mean and fluctuation velocities in Eqs. (27) and (28), we calculate the relative magnitude of the flux term and one of the other two balanced terms in Eq. (15),

$$\frac{|dq/dz|}{|S du/dz|} = \frac{a_2}{2a_3} \left(\frac{d}{h-z} \right)^2. \quad (35)$$

Because the gradient of fluctuation velocity becomes steeper as the free surface is approached, the relative magnitude of the flux term is greatest at the interface between the core and the surface layer. Thus, the relative error is strictly less than $(a_2/2a_3)(d/\ell)^2$. Because the thickness of the surface layer decreases with angle of inclination, the worst error occurs when the angle is small, and it drops with increasing inclination. For example, at the smallest angle of 22° at which Pouliquen [2] observed a deep flow in "system 1," the relative magnitude of the flux term was less than 13%. At the interface with the basal layer, the error at 22° was down to 6% for $h/d=7$ and 0.1% for $h/d=24$. At 28° , the largest error was only 7%. Thus, it is legitimate to neglect the flux gradient term in Eq. (19) to calculate η in the core [Eq. (23)].

V. BASAL FLOW AND MINIMUM HEIGHT

The simulations of Silbert *et al.* [3] clearly reveal the presence of a region above the base consisting of a few layers of grains whose agitation gradually rises from zero at the bumpy boundary to a peak value at the interface with the core. We call this region the "basal layer." Before deriving its governing equations in the following section, it is instructive to consider first its behavior in the limit where the flow height is minimum.

If the height of a deep flow is progressively decreased, as Pouliquen [2] did, then the entire flow eventually reduces to a passive basal layer that possesses no core or surface layer overhead. We call this diminutive flow a "basal flow." Its

height is what Pouliquen [2] called $h_{stop}(\alpha)$.

In basal flows, grains tumble and roll over one another. As Louge and Keast [4] pointed out for thin shear layers near a flat, frictional surface, grains acquire angular momentum from frictional interactions with adjacent granular layers above and below. Thus, the shear stress that a horizontal layer exerts over grains above and below produces angular momentum at a rate \mathbf{P} proportional to the total shear stress and inversely proportional to the moment of inertia I and the grain number density n ,

$$\mathbf{P} \propto S/nI \propto S/\rho_s \nu d^2. \quad (36)$$

Conversely, grains lose angular momentum in collisions with other grains in the same horizontal layer. Because the impact protagonists roll at roughly the same angular velocity, their collisions produce impulses resulting in the frustration of both of their rotation rates. As Louge and Keast [4] showed, the corresponding rate of loss of angular momentum \mathbf{D} is proportional to the collision frequency $\sim \nu g_{12}(\nu) \sqrt{T}/d$ and to the impulsive reduction in granular spin $\sim \sqrt{T}/d$. Then,

$$\mathbf{D} \propto \nu g_{12}(\nu) T/d^2. \quad (37)$$

At steady state, $\mathbf{P} = \mathbf{D}$ or, using Eqs. (14) and (5) through Eq. (9),

$$\frac{S}{N_I} = \frac{\tan \alpha}{1 - \eta \tan \alpha / \mu_E} = C, \quad (38)$$

where C is a constant that we will determine later. At this stage, we will merely assume that C is constant through the depth. Extracting η from this relation, the energy equation becomes

$$\frac{d}{ds} \left(s \frac{dw^*}{ds} \right) - K s w^* = 0, \quad (39)$$

where

$$K = \frac{a_3}{2a_2} - \frac{8C}{a_1 a_2} \left\{ C \left(1 - \frac{\mu_E}{\tan \alpha} \right) + \mu_E \right\}. \quad (40)$$

The form of this differential equation implies that its solutions are Bessel functions. However, because the fluctuation energy flux and, consequently, the slope of w^* must vanish at the free surface, the second kind of Bessel or modified Bessel functions is excluded. Further, because there is no relative velocity between the base and the flowing grains, the flux of fluctuation energy at the bottom boundary is negative and reduces to

$$q = -D, \quad (41)$$

where D is a rate of fluctuation energy dissipation per unit surface of the base. Consequently, because the boundary can only dissipate fluctuation energy with $q \propto -dw/dz \propto dw^*/ds < 0$, the solutions are zeroth-order Bessel functions of the first kind J_0 , with $K < 0$. Defining $m^2 \equiv -K$, these solutions have the form

$$w^* = w_0^* J_0(ms). \quad (42)$$

Using Eq. (40), the condition $K < 0$ implies that there is a minimum angle of inclination for basal flows,

$$\tan \alpha > \frac{\mu_E}{1 - a_1 a_3 / [16C^2] + \mu_E / C}, \quad (43)$$

where the strict inequality indicates that the flow stops altogether as α tends to its lower limit.

The simulations of Silbert *et al.* [3] and the experiments of Pouliquen [2] clearly reveal that basal flows and their deeper counterparts share the same minimum angle of inclination. This is evident by inspecting diagrams showing the heights at which these authors observe SFD flows versus angle of inclination. In these diagrams, the border between the presence and absence of flow is a vertical asymptote at a single minimum angle of inclination. A border having any other shape, such as an oblique asymptote, would have betrayed limiting angles depending on flow depth. Therefore, the minimum angles in Eqs. (24) and (43) are matched. This observation fixes the magnitude of C . From Eq. (38), we then extract the stress fraction in basal flows,

$$\eta = \eta_b = \frac{\mu_E}{\tan \alpha} - \frac{8\mu_E^2}{a_1 a_3}, \quad (44)$$

and, from Eq. (40), the value of $K \equiv -m^2$,

$$m^2 = \frac{a_3}{2a_2} \left\{ 1 - \frac{a_1 a_3}{4\mu_E} \left(\frac{1}{\tan \alpha} - \frac{1}{\mu_E} \right) \right\}. \quad (45)$$

The bottom boundary condition determines the height h_{stop} of basal flows. The simulations of Silbert *et al.* [3] suggest that the fluctuation velocity vanishes at the base, $w = 0$ at $z = 0$. From Eq. (42), this condition implies

$$h_{stop}(\alpha) = j_{01} d / m, \quad (46)$$

where j_{01} is the first root satisfying $J_0(j_{01}) = 0$.

Finally, the condition $0 \leq \eta_b < 1$ must be satisfied for basal flows to exist. We find that any angle $\alpha > \alpha_{min}$ guarantees $\eta_b < 1$. However, to satisfy $0 \leq \eta_b$, Eq. (44) requires

$$\tan \alpha \leq \tan \alpha'_{max} = \frac{a_1 a_3}{8\mu_E}. \quad (47)$$

Curiously, the model thus predicts that the maximum angle for basal flows is larger than the maximum angle for deeper flows, $\alpha'_{max} > \alpha_{max}$. Simulations of Silbert *et al.* [3] will later confirm this peculiar observation.

VI. THE BASAL LAYER

If the height of a basal flow is progressively increased from h_{stop} , then the grain assembly develops a core and a surface layer. Our assumption is that the grains near the base will continue to experience the same stress fraction as in a basal flow [Eq. (44)], and thus to be governed by Eq. (39)

with $K = -m^2$ from Eq. (45). The solution of the energy equation is then

$$w^* = w_1^* J_0(ms) + w_2^* Y_0(ms), \quad (48)$$

where Y_0 is the zeroth-order Bessel function of the second kind. We calculate w_1^* and w_2^* by matching the fluctuation velocity at the interface between the core and the basal layer, and by making it maximum there, $dw^*/ds = 0$. The thickness b of the basal layer is then set by the bottom boundary condition, which we write, once again, $w^* = 0$ at $z = 0$. We find

$$w_1^* = 2 \sqrt{\frac{\Xi_{core} \sin \alpha}{a_1 a_3 v_{core} g_{12}(v_{core})}} \sqrt{\frac{h-b}{d}} \times \frac{Y_0(mh/d)}{Y_0\left(\frac{mh}{d}\right) J_0\left(m \frac{h-b}{d}\right) - J_0\left(\frac{mh}{d}\right) Y_0\left(m \frac{h-b}{d}\right)}, \quad (49)$$

$$w_2^* = -w_1^* \frac{J_0(mh/d)}{Y_0(mh/d)}, \quad (50)$$

and an equation that can be solved for b ,

$$J_0\left(\frac{mh}{d}\right) Y_1\left(m \frac{h-b}{d}\right) = Y_0\left(\frac{mh}{d}\right) J_1\left(m \frac{h-b}{d}\right), \quad (51)$$

where J_1 and Y_1 are the first-order Bessel functions of the first and second kinds, respectively.

We then evaluate the profile of mean velocity by integrating Eq. (20) numerically with $\eta = \eta_b$ subject to $u = 0$ at $z = 0$, and find the value of $u_b^* = u^*(z=b)$ required in Eq. (28). We note that, because w increases from zero at the base, the concavity of the mean velocity profile is opposite to its counterpart in the core (Fig. 3).

Finally, we derive the profile of solid volume fraction from that of the fluctuation velocity using Eq. (21) with $\eta = \eta_b$. As with the core-surface layer interface, there are minor discontinuities at $z = b$ for the solid volume fraction and the velocity gradients, which are the result of the jump of η from η_b to η_{core} (Fig. 4). Once again, these discontinuities are of little consequence for evaluating the overall mass flow rate.

VII. PREDICTIONS

In this section, we compare the predictions of our model with experimental data from Pouliquen [2] and with numerical results from Silbert *et al.* [3]. We begin with the experimental data.

Pouliquen [2] did not measure the frictional or collisional properties of his glass spheres. Instead, he reported the range of inclination angles at which he observed SFD flows. From his minimum and maximum angles, we infer the coefficients of internal friction and normal restitution using Eqs. (24) and (26),

TABLE I. Parameters of Pouliquen's [2] experiments.

System	d (mm)	d_b (mm)	α_{min} (deg)	α_{max} (deg)	e_{eff}	μ_E
1	0.5	0.5	20.7	32.8	0.57	0.42
2	1.3	1.3	21.7	26.4	0.74	0.50
3	1.15	1.3	22.9	30.4	0.64	0.50
4	0.5	1.3	20.9	29.1	0.68	0.44

$$\mu_E = 2 \frac{\tan \alpha_{max}}{\tan \alpha_{min}} [\tan \alpha_{max} - \sqrt{\tan^2 \alpha_{max} - \tan^2 \alpha_{min}}] \quad (52)$$

and

$$e_{eff} = 1 - \frac{2\sqrt{\pi}}{3a_1} \tan^2 \alpha_{max}. \quad (53)$$

The results are summarized in Table I, in which we use $a_1 = 8(1 + \pi/12)/5\sqrt{\pi}$. The relatively high effective restitution justifies our use of Jenkins' expressions [6] for nearly elastic spheres. The internal friction has a magnitude that is typical of granular materials, see, for example, Savage [11].

As Fig. 5 illustrates, our expression for $h_{stop}(\alpha)$ in Eq. (46) captures Pouliquen's measurements for basal flows in system 1. Figure 5 also reveals that, because the heights of nearly all of his deeper SFD flows exceed $\ell + b$, these flows possess a basal layer, a core, and a surface layer.

The theory also confirms the scaling of the depth-averaged velocity that Pouliquen [2] and Silbert *et al.* [3] observed for relatively deep flows. Because the mass flow rates of such flows are dominated by the core region, the principal benchmark for gauging the model's accuracy is to

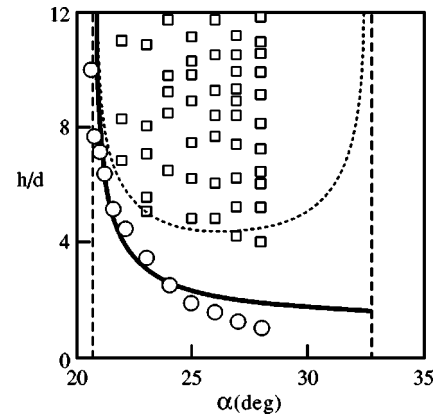


FIG. 5. Dimensionless height of SFD flows versus angle of inclination for Pouliquen's system 1. The circles represent experimental values of h_{stop}/d . The thick solid line is the prediction of Eq. (46). The small squares show the heights of all relatively deep SFD flows observed. The vertical dashed lines show the limiting angles of the core region α_{min} and α_{max} from inequalities (24) and (26). The dashed curve indicates the sum of the heights of the basal and surface layers $\ell(\alpha) + b(\alpha)$. Because our steady, fully developed model assumes the existence of three distinct regions, it ceases to be valid when either the surface layer or the basal layer engulfs the entire flow depth, i.e., when $h < \ell(\alpha) + b(\alpha)$.

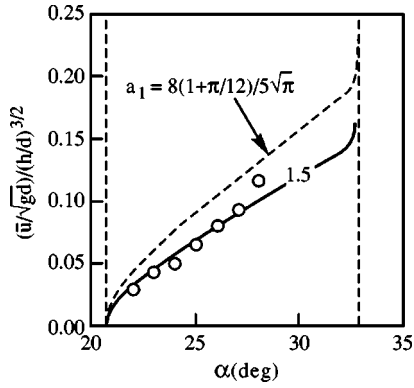


FIG. 6. Ratio $\bar{u}/\sqrt{gd}/(h/d)^{3/2}$ versus angle of inclination. The symbols are measurements with Pouliquen's system 1. The dashed and solid lines are predictions of the model with $a_1 = 8(1 + \pi/12)/5\sqrt{\pi}$ and $a_1 = 1.5$, respectively. Note that, as $\alpha \rightarrow \alpha_{min}$, the core and basal layer disappear, and the remaining basal flow stops.

plot the ratio $\bar{u}/\sqrt{gd}/(h/d)^{3/2}$ versus angle of inclination. As Fig. 6 shows, a model that adopts the constants of Jenkins' theory [6] agrees well with experimental observations. Because these three constants $a_1 = 8(1 + \pi/12)/5\sqrt{\pi}$, $a_2 = 4(1 + 9\pi/32)/\sqrt{\pi}$, and $a_3 = 24(1 - e_{eff})/\sqrt{\pi}$ were derived without considering long-lasting contacts, it is remarkable how well they fare in flows where both rate-dependent and rate-independent stresses coexist. Nearly perfect agreement is obtained using a slightly different value for $a_1 = 1.5$. In Fig. 6, the proximity of the right-most data point to the theoretical dashed curve also hints that a model with the theoretical a_1 works better when the angle of inclination is larger, as expected from a flow with the greatest collisional contribution.

Figure 7 shows the corresponding dependence of the depth-averaged velocity on height and angle of inclination. Note that Pouliquen's system 1 is the only dataset complete enough to permit these comparisons.

Figure 8 shows Pouliquen's measurements of $h_{stop}(\alpha)$ for systems 2, 3, and 4. The model captures data in systems 3

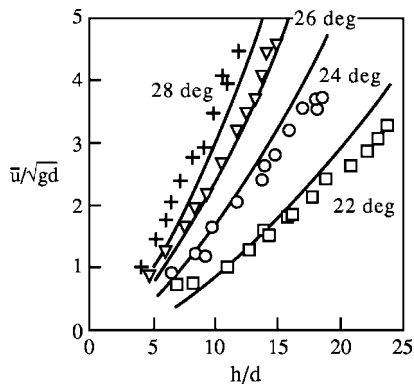


FIG. 7. Dimensionless depth-averaged velocity versus dimensionless flow height for Pouliquen's system 1. The squares, circles, triangles, and crosses represents inclinations of 22°, 24°, 26°, and 28°, respectively. The lines are predictions of the model with $a_1 = 1.5$.

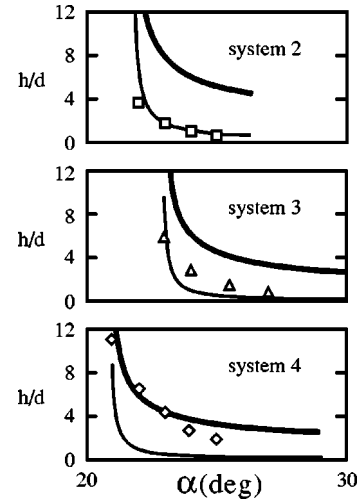


FIG. 8. Dimensionless height of SFD flows versus angle of inclination for Pouliquen's systems 2, 3, and 4. The symbols are experimental values of h_{stop} . The thick and thin solid lines represent $h_{stop}(\alpha)$ from Eq. (46) and $h'_{stop}(\alpha)$ from Eq. (56), respectively.

and 4 reasonably well. However, it clearly overpredicts h_{stop} for system 2. Pouliquen also encountered unexplained difficulties with this system, notably in scaling the depth-averaged velocity. It is possible that for shallow basal flows, the bottom boundary condition may not always be $w=0$ at $z=0$. If the flow was more agitated at the base, then Eq. (41) could be more appropriate. For fully collisional flows, Jenkins and Richman [12] calculated

$$D = 2 \sqrt{\frac{2}{\pi}} (1 - e_w) \frac{1 - \cos \theta}{\sin^2 \theta} N_I \sqrt{T}, \quad (54)$$

where $\sin \theta \equiv (d - d_b + \Delta)/(d + d_b)$ is a measure of the bumpiness of the boundary with spherical bumps of diameter d_b , Δ is the mean separation between the centers of two adjacent bumps, and e_w is the coefficient of normal restitution in the impact of a flow sphere with a bump. Pouliquen's values of d and d_b are found in Table I. We assume that $\Delta = d_b$. If we adopted Eqs. (41) and (54) instead of $w=0$ at $z=0$, then the bottom boundary condition would become

$$\frac{dw^*}{ds} = - \frac{4}{a_2} \sqrt{\frac{2}{\pi}} (1 - e_w) \frac{1 - \cos \theta}{\sin^2 \theta} w^*, \quad (55)$$

and the new flow depth h'_{stop} would satisfy

$$\frac{4}{a_2} \sqrt{\frac{2}{\pi}} (1 - e_w) \frac{1 - \cos \theta}{\sin^2 \theta} J_0 \left(m \frac{h'_{stop}}{d} \right) = m J_1 \left(m \frac{h'_{stop}}{d} \right). \quad (56)$$

Because the solutions of Eq. (39) monotonically decrease with s , h'_{stop} is strictly smaller than h_{stop} in Eq. (46). It so happens that the height of system 2 is more closely predicted by h'_{stop} (thin line, Fig. 8) than it is by h_{stop} . Although basal

flows are too shallow to have much importance in practical applications, it would be useful to investigate their bottom boundary condition further.

An important prediction of our model is that “basal flows” and the “core” region of deep flows do not share the same physics. The former is composed of grains tumbling at a minimum height h_{stop} , below which no flow can exist. The latter is a region, generally deep, where the volume fraction is constant and the production and dissipation of fluctuation energy are nearly balanced. Therefore, in this view, it is a coincidence that the mean velocity of *deep flows*, which is dominated by the core region, should be roughly inversely proportional to the depth h_{stop} of *basal flows*. Pouliquen proposed such empirical relation after analyzing his experimental data, $\bar{u}/\sqrt{gh} \approx \beta(h/h_{stop})$. Although we regard this relation and its “constant” β as coincidental, our model does indicate that it is approximately valid. In fact, we predict that β , despite its relatively weak variations with α , h , μ_E , and e_{eff} , is nearly constant except as it approaches the limits $\alpha \rightarrow \alpha_{min}$ or $h \rightarrow h_{stop}$. For example, for deep flows of Pouliquen’s system 1, we find $\beta = 0.18 \pm 0.03$ for $\alpha \in \{21^\circ, 22^\circ, \dots, 32^\circ\}$, whereas Pouliquen reports $\beta \approx 0.136$. In the limit of “basal flows” where $h \approx h_{stop}$, our model predicts $\beta = 0.063 \pm 0.009$ for $\alpha \in \{21^\circ, 22^\circ, \dots, 32^\circ\}$.

We now turn to the numerical simulations of Silbert *et al.* [3]. These authors considered two kinds of three-dimensional systems that differed in their granular contact laws. The first, labeled “L3,” models contacts using a linear spring-dashpot system tuned to yield a constant coefficient of normal restitution $e = 0.88$. The second, labeled “H3,” assumes a Hertzian contact law with viscoelastic damping that produces a velocity-dependent normal restitution.

Both models assume Coulomb interparticle friction with a coefficient $\mu = 0.5$ independent of relative contact velocity. We do not know how to evaluate the corresponding internal friction coefficient μ_E , in general. However, as the following two-dimensional calculation suggests, we expect a simple relation between μ_E and μ when μ is small. Consider two contacting disks having a line of centers making an angle ξ with the y direction. A force $F_y < 0$ directed along the negative y direction is exerted on the center of mass of the top disk. If μ is small enough for the contact to remain frictional, then the bottom disk opposes a force with projection $F_x = \mu F_y \cos^2 \xi - F_y \sin \xi \cos \xi$ along the x direction. The resulting contribution to internal friction is $\mu' = F_x/F_y$. If all angles ξ have equal probability in the range $-\pi/2 \leq \xi \leq +\pi/2$, then the mean value of μ' is $\mu/2$. Thus, for small μ , we expect $\mu_E \propto \mu$ with $\mu_E < \mu$. In the other limit where $\mu \rightarrow \infty$, we expect that the angle of internal friction should reach an asymptote that is independent of μ .

To evaluate the effective coefficient of restitution from the parameters of the simulations, we invoke the collisional theory of Jenkins and Zhang [10], who provide an expression for $e_{eff} = e_{eff}(e, \mu)$. With $e = 0.88$ and $\mu = 0.50$, they predict $e_{eff} = 0.58$. In general, $e_{eff} < e$.

Figure 9 shows the heights of SFD flows that Silbert *et al.* [3] observed with model L3. From their limiting angles

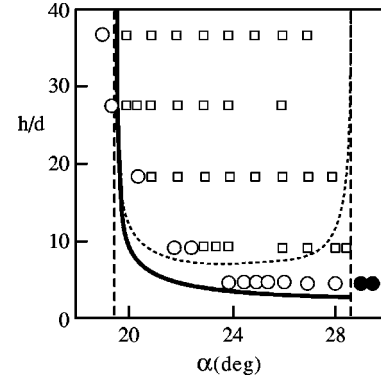


FIG. 9. Dimensionless height of SFD flows versus angle of inclination for the simulations of Silbert *et al.* [3] with model L3. For symbols, lines and comments, see Fig. 5. The solid circles represent basal flows at an angle of inclination that exceeds α_{max} .

$\alpha_{min} = 19.5^\circ$ and $\alpha_{max} = 28.7^\circ$, we infer $\mu_E = 0.40$ and $e_{eff} = 0.83$, which, as expected, are, respectively, smaller than μ and e . In addition, we find that the model agrees well with the data for $h_{stop}(\alpha)$. Finally, the simulations also confirm that steady basal flows can exist with angles of inclination exceeding α_{max} [Eq. (47)], dark circles in Fig. 9.

Figure 10 examines the scaling of the depth-averaged velocity with height and angle of inclination. Unlike the physical experiments of Pouliquen [2], we find that the simulation data depart significantly from the predictions of a model that assumes the constant $a_1 = 8(1 + \pi/12)/5\sqrt{\pi}$ derived from the collisional theory. Instead, we find that $a_1 = 2.1$ captures the data better. However, we note that the magnitudes of the depth-averaged velocities recorded in the simulations of Silbert *et al.* [3] can vary by as much as a factor of 1.8 depending on the form of the contact model employed (models L3 and H3). We also suspect that Silbert *et al.* [3] may have mislabeled some results as L3 rather than H3 in instances mentioned in Figs. 10 and 11.

The principal benefit of the simulations resides with their insight on granular behavior through the flow depth. We find

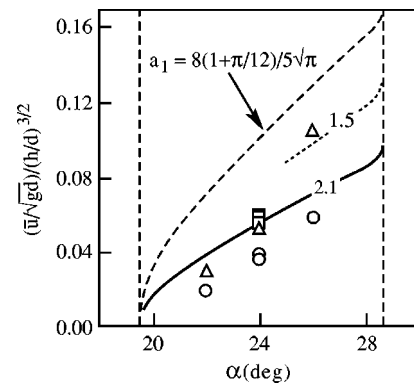


FIG. 10. Ratio $\bar{u}/\sqrt{gd}/(h/d)^{3/2}$ versus angle of inclination. The triangles and circles represent the simulations of Silbert *et al.* [3] for models H3 and L3, respectively. We believe that the squares correspond to model H3, although Silbert *et al.* [3] labeled them as L3. The dashed, dotted, and solid lines are predictions of the model with $a_1 = 8(1 + \pi/12)/5\sqrt{\pi}$, $a_1 = 1.5$, and $a_1 = 2.1$, respectively.

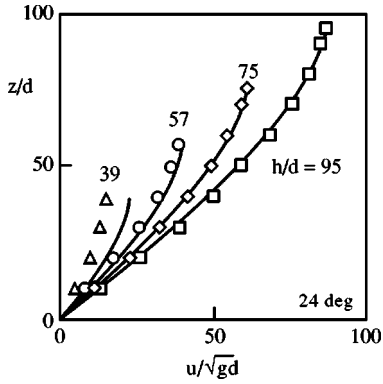


FIG. 11. Profiles of mean velocity versus depth at an inclination of 24° and for the relative heights shown. The lines are predictions of the model with $a_1=2.1$. The squares, diamonds, and circles are for model *L3* of Silbert *et al.* [3]. We suspect that the triangles belong instead to model *H3*, which would explain the unexpected discrepancy between model and data at $h/d=39$.

that our model closely captures the profiles of mean and fluctuation velocity reported by Silbert *et al.* [3]. Figure 11 shows mean velocity profiles for several flow heights. Unfortunately, because Silbert *et al.* [3] only reported relative profiles of fluctuation velocity, we could not evaluate the degree of anisotropy of their velocity fluctuations or compare these with absolute predictions of our model. Nonetheless, as Fig. 12 illustrates, the model reproduces relative profiles of fluctuation velocity well.

Finally, Silbert *et al.* [3] examined the dependence of the mean flow rate on interparticle friction μ and normal restitution e at $\alpha=22^\circ$. To compare our predictions with their results despite the absence of data for μ_E and e_{eff} , we adopt the theory of Jenkins and Zhang [10] for the effective restitution, and we assume that the ratio μ_E/μ remains constant and equal to the value 0.40/0.50 that we determined earlier. As Fig. 13 shows, this approach captures well the dependence of the mean flow rate on friction when μ is small. At higher values, the mean flow rate becomes independent of μ as μ_E reaches a constant asymptotic value. Further, the

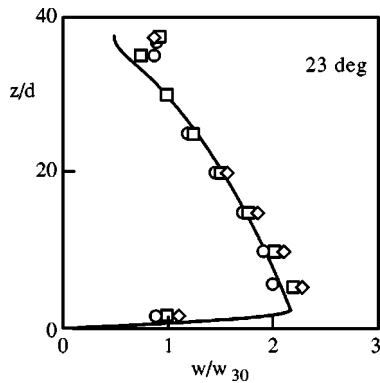


FIG. 12. Relative profiles of fluctuation velocity versus depth at an inclination of 23° . The abscissa is w relative to its value w_{30} at $z/d=30$. The lines are predictions of the model with $a_1=2.1$. The squares, diamonds, and circles are the data of Silbert *et al.* [3] for model *L3* in the x , y , and z directions, respectively.

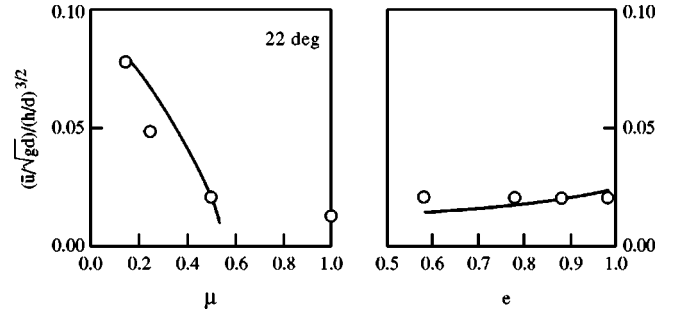


FIG. 13. Ratio $\bar{u}/\sqrt{gd}/(h/d)^{3/2}$ versus interparticle friction and normal restitution for an inclination of 22° and $h/d=40$. The symbols represent the simulations of Silbert *et al.* [3] for models *L3*. The lines are predictions of the model with $a_1=2.1$, $\mu_E/\mu=0.80$, and $e_{eff}=e_{eff}(\mu,e)$ from Jenkins and Zhang [10].

model clearly agrees with Silbert *et al.* [3] that the flow rate is much more sensitive to interparticle friction than it is to normal restitution (Fig. 13). Because purely collisional theories ($\eta=0 \forall v$) predict instead that $\bar{u}/\sqrt{gd}/(h/d)^{3/2}$ depends strongly on e and weakly on μ , their relevance to dense SFD flows down a bumpy incline is questionable.

VIII. CONCLUSIONS

We have outlined a model for granular flows down bumpy inclines in which the stresses have a collisional, rate-dependent part coexisting with a rate-independent, frictional contribution [5]. For deep flows, the model distinguishes three regions: a basal layer where grains gradually acquire fluctuation kinetic energy away from the base; a core where the solid volume fraction is constant; and a collisional surface layer, where the volume fraction decreases rapidly near the free surface. The model also describes the behavior of basal flows, which possess the smallest sustainable height.

With insight from the numerical simulations of Silbert *et al.* [3], we have proposed simple closures for the governing equations of SFD flows in the three regions. The resulting solutions provided expressions for the limiting angles at which such flows exist, and for the profiles of mean and fluctuation velocities through the depth. They also predicted the scaling of the mean flow rate with angle of inclination and flow height.

Although our results compared favorably with the physical experiments of Pouliquen [2] and the numerical simulations of Silbert *et al.* [3], several issues warrant further research. Foremost, it remains to explain why the solid volume fraction remains constant in the core, and to predict its value without resorting to an empirical closure. It is possible, for example, that the constant volume fraction may be associated with a phase transition between two states in which collisional and enduring stresses, respectively, dominate.

In this context, related work should focus on deriving constitutive relations for rate-dependent stresses and collisional boundary conditions that account explicitly for the presence of enduring contacts. In addition, the angle of internal friction should be calculated in terms of frictional

properties of the contacts, or related to other physical parameters, such as the angle of repose, so that limiting angles for SFD flows can be predicted from independent measurements.

Another opportunity for research is to reexamine the closure in the basal layer of deep flows, or in basal flows of a minimum height. If, as we suggest, the angular momentum of the grains plays an important role there, then it may be fruitful to extend the micropolar fluid theory of Hayakawa [13] and Mitarai *et al.* [14] from purely collisional flows to granular flows experiencing enduring contacts as well.

Finally, the numerical simulations should be interrogated further to examine whether the model correctly predicts the

absolute level of fluctuation velocity, and to inform the development of a better model.

ACKNOWLEDGMENTS

This work was supported by NASA Grant Nos. NCC3-468 and NAG3-2112, and by the International Fine Particle Research Institute. The author gratefully acknowledges the help of Haitao Xu and the benefit of discussions with Patrick Richard, Renaud Delannay, Alexandre Valance, Luc Oger, James Jenkins, Deniz Ertas, Leonardo Silbert, Thomas Halsey, James Landry, and Gary Grest. He is also grateful for the financial support of the Université de Rennes for his visits there during the summers of 1998, 1999, 2000, and 2002.

-
- [1] O. Pouliquen and F. Chevoir, *C. R. Physique* **3**, 163 (2002).
 - [2] O. Pouliquen, *Phys. Fluids* **11**, 542 (1999).
 - [3] L. Silbert, D. Ertas, G. Grest, T. Halsey, D. Levine, and S. Plimpton, *Phys. Rev. E* **64**, 051302 (2001).
 - [4] M. Louge and S. Keast, *Phys. Fluids* **13**, 1213 (2001).
 - [5] S. Savage, in *Mechanics of Granular Materials—New Models and Constitutive Relations*, edited by J. Jenkins and M. Satake (Elsevier, New York, 1983), pp. 261–282.
 - [6] J. Jenkins, *Hydraulic Theory for a Debris Flow Supported on a Collisional Shear Layer* (IAHR, Tokyo, 1993), pp. 1–12.
 - [7] C. Campbell, *J. Fluid Mech.* **465**, 261 (2002).
 - [8] S. Torquato, *Phys. Rev. E* **51**, 3170 (1995).
 - [9] N. Carnahan and K. Starling, *J. Chem. Phys.* **51**, 635 (1969).
 - [10] J. Jenkins and C. Zhang, *Phys. Fluids* **14**, 1228 (2002).
 - [11] S. Savage, *J. Fluid Mech.* **92**, 53 (1979).
 - [12] J. Jenkins and M. Richman, *J. Fluid Mech.* **171**, 53 (1986).
 - [13] H. Hayakawa, in *Traffic and Granular Flow 2001*, edited by Y. Sugiyama and D. Wolf (Springer, New York, in press).
 - [14] N. Mitarai, H. Hayakawa, and H. Nakanishi, *Phys. Rev. Lett.* **88**, 174301 (2002).